Environmental Science Advances

ROYAL SOCIETY OF CHEMISTRY

PAPER

View Article Online
View Journal | View Issue

Cite this: *Environ. Sci.: Adv.*, 2025, **4**, 115

Porosity and fluid pathway development during cadmium sequestration by calcium carbonate replacement†

Maude Julia, *[a] Christine V. Putnis,[ab] Oliver Plümper[c] and François Renard[de]

Cadmium contamination of ground water and soil has drastically increased in some areas through the last few decades and remediation strategies are currently being investigated. The coupled dissolution–precipitation of calcium carbonate in cadmium-containing solutions leads to the precipitation of a $(Ca,Cd)CO_3$ phase of lower solubility, this process trapping cadmium from a solution into a solid phase. The present study analyses the reactions of two types of calcium carbonates (calcite as Carrara marble and aragonite) in cadmium solutions and compares the different reaction pathways and their respective efficiency. X-ray tomography scans of different Carrara marble and aragonite samples reacted in cadmium solutions for 16 to 64 days at 200 °C were acquired and analysed. The reaction in Carrara marble proceeds through a dissolution–precipitation reaction from the surface of the sample. The fluid moves through the porosity developed in the newly precipitated phase and along grain boundaries. Tomograms show that the porosity at the post-reaction time of imaging is mainly disconnected and that the reaction extent decreases with an increase in cadmium concentration of the solution. For aragonite, the main reaction pathway is opened by reaction-induced fracturing, which leads to a faster reaction than for the Carrara marble as the reaction pathways open faster towards the centre of the sample through successive hierarchical fracturing. The reaction rate for aragonite increases with time and cadmium concentration of the solution. Thus, the sequestration of cadmium from solution is potentially more efficient using aragonite due to the reaction-induced fracturing process taking place.

Received 15th August 2024
Accepted 16th October 2024

DOI: 10.1039/d4va00316k

rsc.li/esadvances

Environmental significance

Heavy metal contamination of soil and ground water caused by anthropogenic activities has increased in the last few decades and has become a real concern in some areas. Cadmium in one of these contaminant elements and its toxicity for humans through long term exposure has been shown to cause heavy renal and bone diseases. Our study focuses on the use of carbonate rocks as remediation materials as these are widely available and their reaction with cadmium-containing solutions can lead to the precipitation of less soluble phases containing cadmium through a coupled dissolution–precipitation mechanism. The study of the mechanisms of cadmium uptake by different carbonate materials will provide a base for the development of better remediation strategies.

Introduction

Environmental pollution of surface waters has been steadily increasing in the years since industrialization mainly through anthropogenic activities, including mining, agriculture, industrial and pharmaceutical manufacturing processes. This leads to heavy metal water and soil pollution[1–6] as well as excess phosphates[7] from agricultural applications, causing eutrophication of waterways,[8] and excess atmospheric CO_2.[9] Consequently, there is an increasing need to mitigate this contamination by sustainable methods using available and affordable materials. Many recent research activities are focusing attention on suitable methods to tackle toxic element contamination. Coupled dissolution–precipitation reactions have been studied as a potential means to remediate environmental pollution. Toxic elements such as Pb,[10–12] Se,[13–15] As,[14,16] Sb,[14,17] Cr,[18] and Cd[19–26] have all been studied to suggest potential decontamination strategies using dissolution–precipitation processes that involve minerals. Amongst the examples of pollution already cited, increasing soil and water cadmium (Cd) pollution has been a reason for concern in some regions.[4,5] Anthropogenic cadmium pollution originates from

[a]*Institut für Mineralogie, Universität Münster, Corrensstrasse 24, 48149 Münster, Germany. E-mail: mjulia@uni-muenster.de*
[b]*School of Molecular and Life Sciences, Curtin University, Perth, 6845, Australia*
[c]*Department of Earth Sciences, Universiteit Utrecht, 3584 CB Utrecht, the Netherlands*
[d]*The Njord Centre, Departments of Geosciences and Physics, University of Oslo, Oslo, Norway*
[e]*ISTerre, Univ. Grenoble Alpes, Grenoble INP, Univ. Savoie Mont Blanc, CNRS, IRD, Univ. Gustave Eiffel, 38000 Grenoble, France*

† Electronic supplementary information (ESI) available. See DOI: https://doi.org/10.1039/d4va00316k

activities such as non-ferrous metal mining, the intensive use of phosphate fertilizers or the disposal of municipal waste.[27] Long term exposure to cadmium can lead to serious health problems such as osteomalacia and renal tubular failure.[28–30] This has promoted the need to find remediation strategies to sequester cadmium from the soil and surface water.[31–33]

Coupled dissolution–precipitation reactions allow the precipitation of a stable mineral phase, containing the target toxic element, through the dissolution of a parent mineral with a higher solubility in a contaminated solution. During a replacement reaction, if the difference in molar volumes of the parent and final phases, as well as their relative solubilities allows a reaction to proceed, this reaction can lead to the complete pseudomorphic replacement of the parent mineral.[34] Additionally, for a pseudomorphic replacement to be complete, the new phase must provide a pathway for the fluid to reach the reaction interface with the parent material such as connected porosity, grain boundaries or fracture networks. Some coupled dissolution–precipitation reactions have been observed to lead to a complete pseudomorphic replacement of the parent material.[35,36]

Carbonates, such as limestone, dolomite, and marble, are common rocks in the crust of the Earth and their relative solubility and crystal structure allow for reactions with multicomponent aqueous solutions to result in the formation of a new more stable (less soluble) phase. Therefore, reactions with carbonates present a viable possibility of achieving some acceptable degree of environmental remediation.[10,11,13,16–18,37]

The present study focuses on the replacement reactions between carbonates and solutions containing dissolved cadmium. Due to the existence of an ideal solid solution between calcite ($CaCO_3$) and otavite ($CdCO_3$),[38,39] coupled dissolution–precipitation reactions have been investigated between $CaCO_3$ and cadmium-containing solutions as a potential cadmium trapping strategy. As otavite has a slightly lower molar volume than both calcite and aragonite[21] a potential replacement of the $CaCO_3$ sample could be reached. Experiments have shown that the surfaces of calcite single crystals are passivated by cadmium in solution due to the epitaxial growth of a $CdCO_3$ layer on the crystal surface.[22,24] This is due to the similar crystallographic structure and lattice parameters of $CaCO_3$ and $CdCO_3$ as well as the lower solubility of $CdCO_3$ compared to $CaCO_3$. Our previous study[21] showed that by using polycrystalline calcite (such as marble) or a polymorph of calcite (such as aragonite) a partial replacement of $CaCO_3$ by a (Ca,Cd)CO_3 solid solution could be achieved. The presence of grain boundaries and random orientation of the calcite grains in the case of Carrara marble have allowed the initial material to dissolve and be replaced with a porous (Ca,Cd)CO_3 solid solution probably by hindering the epitaxial growth of otavite onto the calcite surface[22] and facilitating access of the fluid into the sample. As the new precipitating phase has a lower molar volume and identical crystallographic structure to calcite, the replacement is pseudomorphic and does not cause fracturing of the sample. The replacement proceeded more efficiently from the surface than from the grain boundaries in the Carrara marble samples. In the case of aragonite during the reaction with a cadmium-containing solution, the change of crystallographic structure and subsequent interfacial stresses induced fracturing of the samples during the replacement reaction, allowing fluid penetration and replacement inside the sample. Reaction-induced fracturing has been observed and studied previously, showing that it could in some cases sustain a replacement reaction or inhibit it.[40–44] However, all observations were made on two-dimensional images of sample sections and the progression of the reaction with time and solution concentration could not be quantified. More information about the reaction extent for both materials as well as their dominant fluid pathways is required to determine which material and type of reaction are more efficient for cadmium-sequestration from solution. This high pressure and temperature reaction could provide a potential method for water decontamination in industrial settings as well as a starting point to extend research on experimental conditions closer to an environmental setting.

In order to study the extent of the reaction for both aragonite and Carrara marble (calcite) we have reproduced some of the reactions from Julia *et al.*[21] and analysed the resulting samples using 3D X-ray tomography imaging. Both aragonite and Carrara marble samples were reacted in cadmium solutions for different durations and solution concentrations and scanned by X-ray microtomography to obtain 3D X-ray adsorption tomograms. These tomograms were then compared to assess the extent of the reaction, development of porosity and potential fluid pathways, depending on the sample type, reaction time and solution composition.

Methods

Sample preparation

Cubes of Carrara marble (Italy), with dimensions of $3 \times 3 \times 3$ mm^3, consisting of compacted calcite grains, with an average size of approximately 300 μm, with randomly oriented grain boundaries, were cut with a saw from a single marble block in the absence of water, following the method of Julia *et al.*[21] Crystals of aragonite (Molina de Aragón, Spain) were broken into 2–3 mm wide pieces. The purity of the starting materials was assessed by X-ray diffraction (the XRD spectra of the starting materials are available as ESI Fig. S1 and S2†).

Solutions with cadmium concentrations of 0.4 M and 2 M were prepared with technical grade $CdCl_2$ (99%, Fisher Scientific) dissolved in deionized water (resistivity > 18 mΩ cm). The pH of the solutions was measured with an Inolab pH/ION Level 2 pH meter and calculated with PHREEQC.[45]

The samples were reacted at 200 °C for 16, 32 or 64 days in a 0.4 or 2 M $CdCl_2$ solution. 3 mL Teflon sample holders were filled with 2 mL of solution, with the sample and sealed in brass cylinders. The autogenous pressure reached in the sample holders during the reaction can be estimated to be equal to the vapor pressure, so 16 bars. After reaction the samples were cooled in a stream of compressed air, dried and imaged by X-ray microtomography.

X-ray microtomography acquisition

The acquisition of the X-ray microtomography scans for the Carrara marble samples after different durations of reactions

was conducted at the beamline BM05 at the European Synchrotron Radiation Facility (ESRF) in Grenoble, France. Each Carrara marble sample was scanned at the beamline BM05 at ESRF, using a pink beam (*e.g.*, white beam with two filters of 6.67 mm of aluminium and 20 mm of SiO_2). For each volume, 2999 radiographs were acquired over a rotation of 360 degrees. The duration of each scan was 4 minutes. The volumes were reconstructed using phase contrast as in Mirone *et al.* (2014).[46] The spatial resolution of the 3D tomograms is between two and three times the voxel size.

The aragonite samples were scanned at the EPOS-NL MINT facility, Utrecht University, the Netherlands, with a Zeiss Xradia 610 Versa X-ray tomography microscope system equipped with a 160 kV X-ray source. A full volume of each sample was acquired with the voxel size necessary to attain full visualization of the sample. Four higher resolution scans were acquired in specific areas of some of the samples. The spatial resolution of the 3D tomograms is between three and five times the voxel size. The specifications of the different scans are provided in Table 1.

Data segmentation and analysis

The segmentation of the reacted Carrara marble cube dataset was conducted with the software Ilastik 1.3.3.[47] The software was trained on 100 images to analyse a stack of 1000 images of each tomogram and separate the following phases: the background, the solid solution (the replaced phase of the samples), the remaining calcite, and the pores. Each of the 100 training images was manually segmented until the phase separation was completed before feeding the remaining images to the software for automatic segmentation. The top and bottom face of the samples were excluded to ensure a consistent segmentation by feeding the software with similar images. An example of the segmentation outcome is given in Fig. 1.

The segmented Carrara marble datasets were then analysed using the software Thermo Scientific Avizo 3D 2023.1. Potential areas of phase misattribution were manually corrected and the volume of the respective phases was extracted as well as the porosity connectivity. In addition, the pore volume repartition was obtained using the software Dragonfly during re-examination of the dataset. After extraction of the volumes of the different segmented phases, the results were extrapolated to represent the full cube, instead of the analysed slice. This assumes that the reaction has the same behaviour on all faces of the cube.

The reacted aragonite samples were segmented by grey-scale separation with the software Avizo 3D. The porosity could not be separated due to the combination of the pores small size and the limited resolution of the images. Only three phases were identified: the background, the solid solution (reacted sample) and the remaining aragonite.

Efficiency of the segmentation

As visible in Fig. 1(B) and (E), some areas of the Carrara marble samples segmented with Ilastik 1.3.3 are attributed to the wrong phase due to some shadow effects and closeness of grey levels present in the original dataset. Most of these misattributions consisted of some background attributed as calcite on the sides of the samples and spots of background falsely detected inside the samples. These artefacts were manually corrected during analysis and reattributed to the correct phase. A comparison of the different steps of the segmentation is shown in Fig. 1. The segmentation showed other limitations such as the non-separation of the crystals of $CdCl_2$ precipitated on the surface

Table 1 List of experiments, X-ray microtomography scan condition summary, and samples prepared for SEM analyses

Sample type (X-ray imaging)	Reaction conditions	Sample name	Scan type	Voxel size (μm)	Additional sample prepared for SEM
Carrara marble (ESRF, beamline BM05)	16 days – 0.4 M $CdCl_2$	Carrara – 01	Full sample	2.3	Yes
			Zoom	0.36	
	32 days – 0.4 M $CdCl_2$	Carrara – 02	Full sample	2.3	Yes
			Zoom	0.36	
	64 days – 0.4 M $CdCl_2$	Carrara – 03	Full sample	2.3	Yes
			Zoom	0.36	
	16 days – 2 M $CdCl_2$	Carrara – 04	Full sample	2.3	Yes
			Zoom	0.36	
	32 days – 2 M $CdCl_2$	Carrara – 05	Full sample	2.3	Yes
			Zoom	0.36	
	64 days – 2 M $CdCl_2$	Carrara – 06	Full sample	2.3	Yes
			Zoom	0.36	
Aragonite (Zeiss Xradia 610 Versa)	16 days – 0.4 M $CdCl_2$	Aragonite – 01	Full sample	5.5	No
			Zoom	0.43	
	32 days – 0.4 M $CdCl_2$	Aragonite – 02	Full sample	5.5	Yes
			Zoom	0.8	
	64 days – 0.4 M $CdCl_2$	Aragonite – 03	Full sample	5.5	Yes
			Zoom	0.43	
			Zoom	0.43	
	16 days – 2 M $CdCl_2$	Aragonite – 04	Full sample	6.7	No
	32 days – 2 M $CdCl_2$	Aragonite – 05	Full sample	6.7	Yes
	64 days – 2 M $CdCl_2$	Aragonite – 06	Full sample	6.7	No

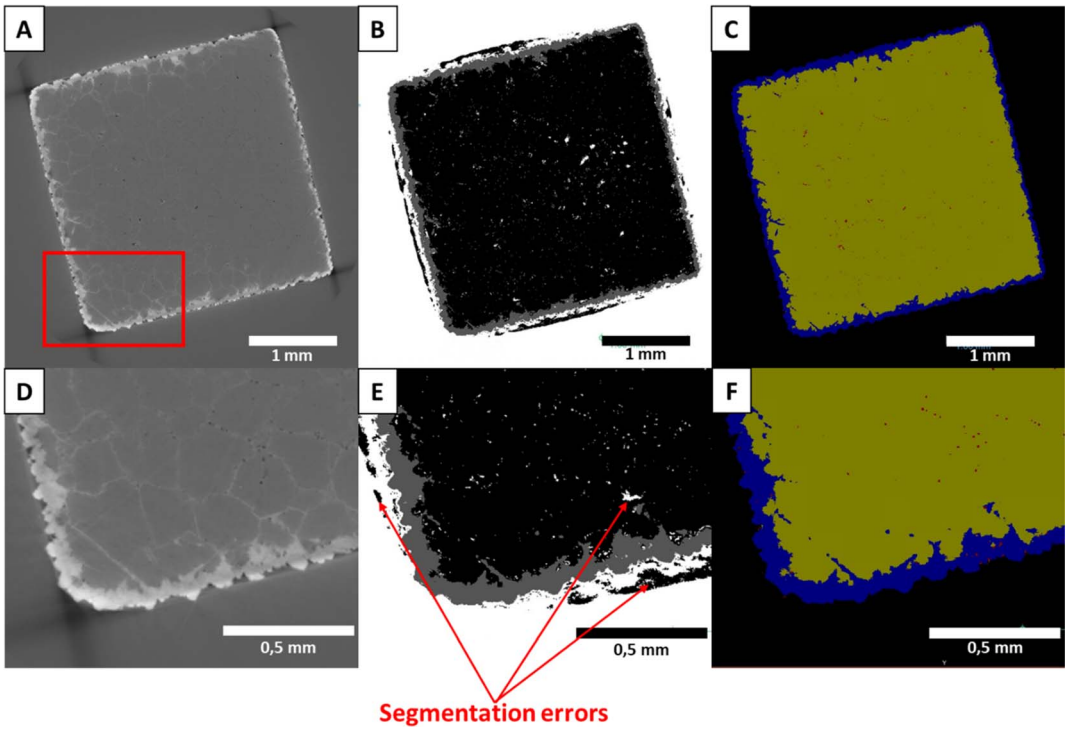

Fig. 1 X-ray tomography imaging of marble sample Carrara-04 reacted for 16 days in 2 M $CdCl_2$: (A) original slice, (B) after segmentation with the software Ilastik (white: background, dark grey: $(Ca,Cd)CO_3$ solid solution, light grey: pores, black: calcite) and (C) after attribution of the phases (yellow: calcite, blue: $(Ca,Cd)CO_3$ solid solution, red: pores, black: background) and correction of the segmentation errors. (D–F) are zooms into respectively (A–C) (zoom area is shown by the square in A). The reaction progressed by the formation of a rim of solid solution around the original carbonate cube and by reaction along the grain boundaries. The reaction product at the grain boundaries could not be segmented due to the limited resolution of the images.

of the sample during quenching of the reaction from the rest of the solid solution created by the replacement of the original material (SEM images of a reacted Carrara marble sample with highlighted $CdCl_2$ crystals are available as ESI Fig. S3†). Moreover, the mineral replacement observed along the grain boundaries could not be segmented due to the low difference of grey level between the replaced phase and the original material combined with the thinness of the replacement along the grain boundaries. After thorough examination of the sample scans and their segmentation, it was concluded that only the thin (<5 μm) replacement layer along the grain boundaries was unsegmented and no larger replaced area had been omitted. Both these segmentation limitations were consistent within the dataset and deemed not to hinder the comparison of the samples.

For the aragonite dataset, the crystals of $CdCl_2$ precipitated on the surface (SEM image of an aragonite sample with highlighted $CdCl_2$ crystals is available as ESI Fig. S4†) could not be separated from the rest of the replaced area as their colours on the grey level scale are overlapping and no specific shape/delimitation mark could provide a good ground for other segmentation methods such as watershed segmentation or the Ilastik 1.3.3 software. The porosity present in the samples could also not be segmented to a separate phase. Most of the porosity was segmented with the replaced phase, as shown in Fig. 2.

Scanning electron microscopy and elemental analysis

Additional aragonite and Carrara marble samples were reacted under similar conditions to those analysed by X-ray microtomography and were embedded in epoxy resin and cut through the centre. They were then carbon coated and observed by scanning electron microscopy (SEM) and energy-dispersive spectroscopy analysis. The reaction conditions used for these samples are shown in Table 1.

Results

Extent of the reaction

The volumes of the replaced phase and remaining original material were extracted for all samples and are plotted against each other in Fig. 3.

The data show that the replacement of the samples during the reaction is more advanced at equal time and solution concentration for the aragonite samples than for the Carrara marble samples (Fig. 3). The Carrara marble dataset shows that the reaction keeps progressing with time for both solutions tested. A slowing of the reaction is visible when the solution concentration is increased. The aragonite samples show little reaction progression between samples reacted for 16 and 32 days and a larger gap between samples reacted for 32 and 64 days. An increase in the solution concentration leads to a higher replacement rate and widens the gap between the samples

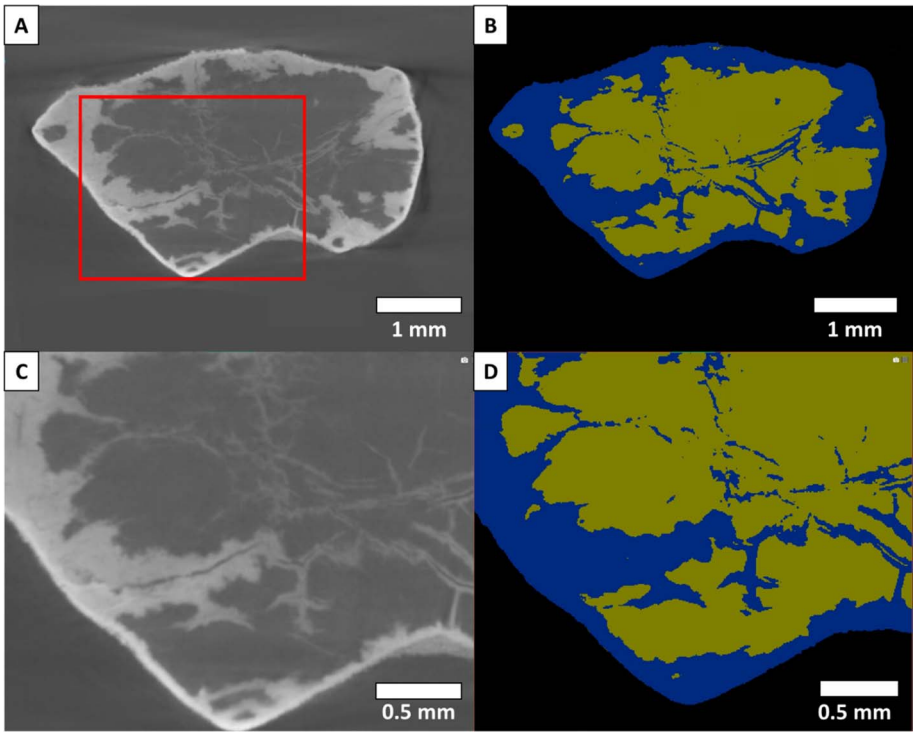

Fig. 2 X-ray tomography imaging of sample Aragonite-04 reacted for 16 days in 2 M $CdCl_2$: (A) original X-ray tomography slice, (B) after segmentation (yellow: aragonite, blue: solid solution of $(Ca,Cd)CO_3$, black: background). (C and D) are zooms into respectively (A and B), the zoom area is indicated by the red area in A. The transformation of aragonite into a solid solution that contains cadmium occurred by a process of reaction-induced fracturing.

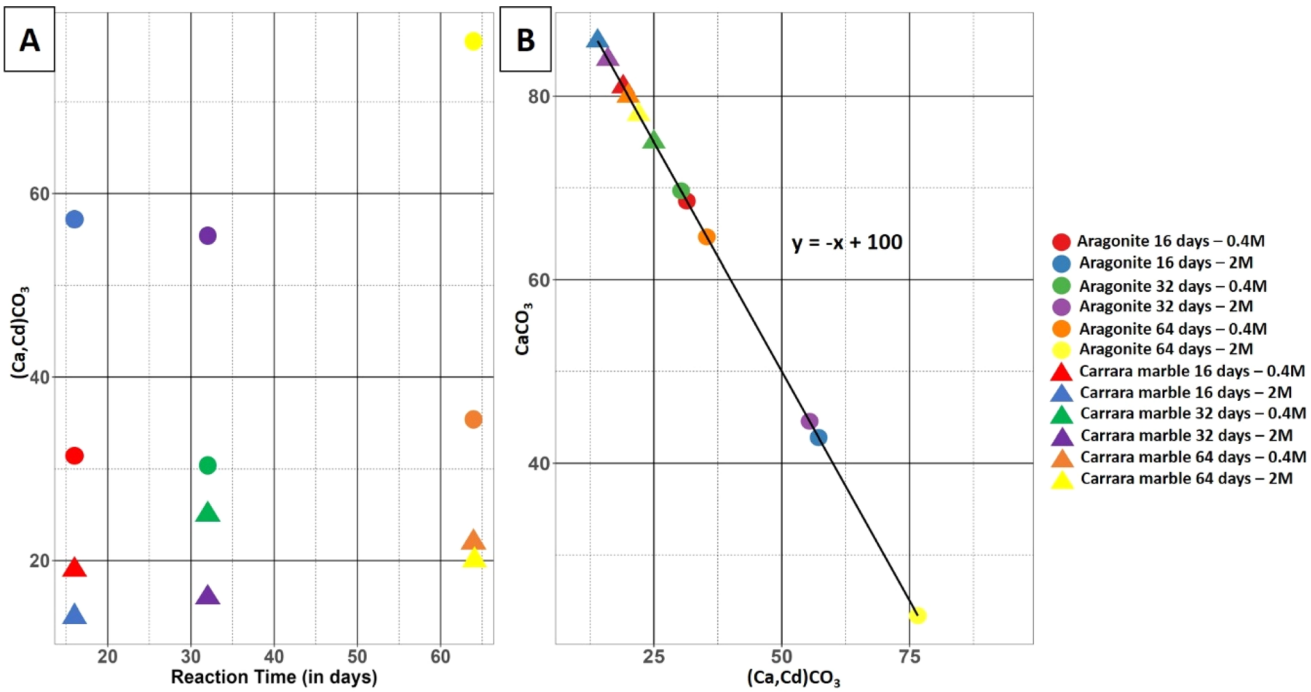

Fig. 3 (A) Evolution of the volume of the replacement phase $(Ca,Cd)CO_3$ as a function of reaction time for both datasets and concentrations of cadmium in solution, (B) phase volume comparison of the replacing phase $(Ca,Cd)CO_3$ vol%) against the remaining original material ($CaCO_3$ vol%) for the reacted Carrara marble and aragonite datasets. The linear trend with a slope of −1 indicates volume conservation of the solid during replacement. The legend on the right side of the figure is a common legend for both figures (A and B).

reacted for 32 and 64 days. The replacement can be divided in two categories: the replacement progressing inside the sample through reaction-induced fracturing and the replacement layer on the sample surface. The thickness of the replaced layer along the sample surface was measured for samples Aragonite-01 to Aragonite-05 using the X-ray microtomography scans, as displayed in ESI Fig. S5† with the measurement value and its standard deviation for each sample. Sample Aragonite-06 presented too many fractures and a too advanced replacement to separate areas where the replacement progressed from fractures starting from the outer surface. One hundred measurements were taken from three cross-sections on each sample, carefully selecting areas as far as possible from fractures to avoid reaction interference. An example image of the thickness measurement of the surface replacement in an aragonite sample is provided in Fig. S6.† A slight increase in the layer thickness could be observed with increasing time of reaction for the samples reacted in 0.4 M $CdCl_2$ solution as well as with an increase in cadmium concentration in the solution. This increase of thickness with reaction time was not consistent for the samples reacted in a 2 M $CdCl_2$ solution, however the third sample of this set could not be used for comparison and sample specificities could have influenced the surface reaction.

Porosity and connectivity

The porosity volume was extracted from the full scans of the Carrara marble dataset. A three-dimensional rendering of the porosity and the replaced area is shown in Fig. 4. The segmented pores represent less than 1% of the volume of each sample with no specific trend related to the reaction time and/or the solution concentration. The minimum pore size extracted for each sample was 10 μm^3 and was limited by the segmentation method efficiency to detect small pores. The majority of the pores had a volume of the order of 10–100 μm^3 (ESI Fig. S7† shows the pore size distribution for each Carrara marble sample). The pore connectivity was analysed from both the full scans and the zoom scans. Mostly the porosity was disconnected at the spatial resolution of the images and at the time when the scans were acquired (1–2 months after the end of the reaction).

The porosity of the replaced phase in the aragonite dataset could not be segmented from the rest of the material. SEM images of a reacted aragonite sample sectioned through the middle were used to gather information about the porosity in the replaced phase. Fig. 5 shows the morphology of the replacement along newly formed fractures and a thin layer of replacement on the sides of the samples. The zoom in Fig. 5(B) shows that the thin layer of replacement along the sample surface is porous, although not being the area with the most replacement. The size of the pores visible by SEM in the aragonite sample goes down to ~0.5 μm. SEM images of the porosity in both Carrara marble and aragonite samples reacted under similar conditions is available in the ESI as Fig. S8† as visual comparison.

Discussion

This study compares the extent and mechanism of the coupled dissolution–precipitation reaction of two different forms of $CaCO_3$, Carrara marble consisting of compact calcite grains and single aragonite crystals, in cadmium-containing solutions leading to the precipitation of $(Ca,Cd)CO_3$ solid solutions for different partial pseudomorphs of $CaCO_3$. The extent of the reaction was more advanced for the aragonite samples than for the Carrara marble samples, for the same reaction conditions (Fig. 3). This difference may be explained by the different types of pathways used by the fluid to reach the unreacted material for the two types of samples and the small difference of solubility between calcite, $-\log K_C = 11.47$ at 200 °C, and aragonite, $-\log K_A = 11.28$ at 200 °C.[48]

In the case of Carrara marble, it has already been shown that fluid can penetrate along the grain boundaries and through newly formed connected porosity in the replaced areas.[21,35,49,50] The respective molar volumes of calcite (36.93 $cm^3\ mol^{-1}$) and otavite (33.97 $cm^3\ mol^{-1}$)[21] are quite close and show that the replacement of calcite by otavite or a $(Ca,Cd)CO_3$ solid solution is not optimal for the creation of porosity. The analysis of the porosity inside the reacted Carrara marble samples, after segmentation of X-ray tomograms, does not show any

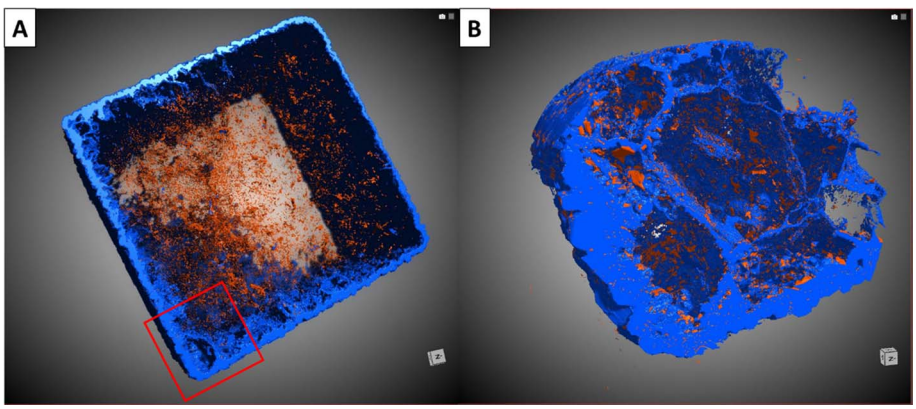

Fig. 4 Synchrotron tomography rendering of the marble sample Carrara-04 reacted for 16 days in a 2 M $CdCl_2$ solution. The replaced phase appears in blue and the porosity is in red. (A) Full cube with a voxel size of 2.3 μm and (B) a corner of the same sample with a voxel size of 0.36 μm showing both the external reaction rim and some reaction product along grain boundaries. From these data, the reacted volume is calculated.

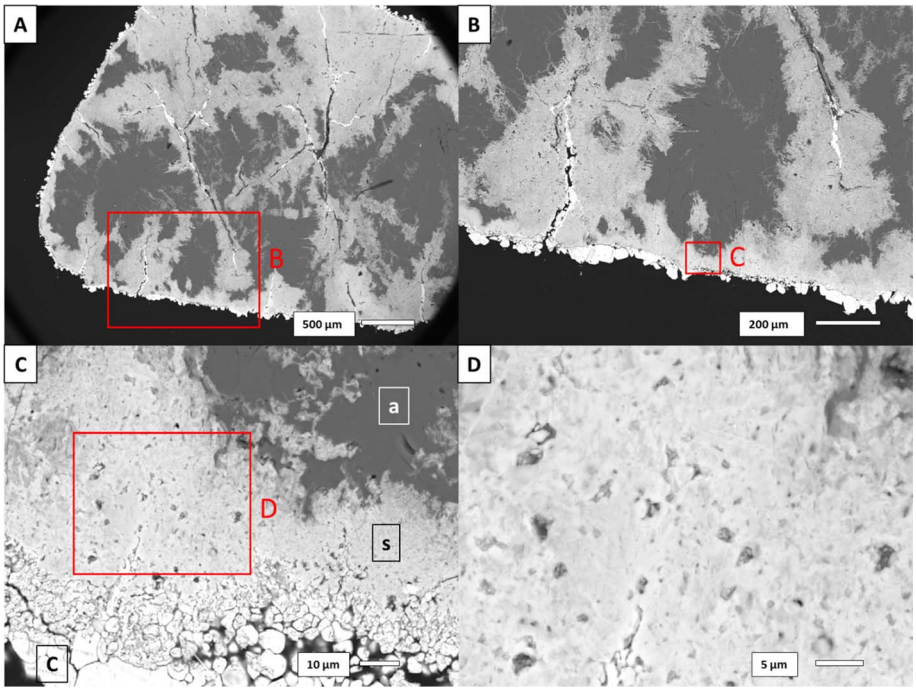

Fig. 5 Back-scattered electron images of sample Aragonite-03 reacted for 64 days in a 0.4 M $CdCl_2$ solution with (A) the full sample and (B–D) are consecutive zooms in the areas indicated in red in the previous images. The labels in C indicate the different phases are: (a) aragonite, (s) the $(Ca,Cd)CO_3$ solid solution and (c) the $CdCl_2$ crystals.

connectivity at the resolution of the tomograms acquired in the present study. However, the advancement of the reaction through time observed in Fig. 3 suggests that fluid pathways allowed the reaction to progress. It is possible that the cooling process of the samples before imaging caused a reequilibration of the pore space leading to the disappearance of pore connectivity through the minimising of surface area. Textural reequilibration during a replacement reaction is driven by a reduction of surface energy and can result in a loss of pore connectivity.[36] X-ray tomography was carried out several weeks post experiments giving time for loss of pore connectivity. Moreover, the porosity analysed is the result of the segmentation of the scans and porosity with a size smaller than the resolution of the segmentation (<0.5 µm) could not be imaged, causing a loss of information concerning nanopores. Smaller pores have probably been present and have provided a pathway for the fluid towards the centre of the sample. Furthermore it has been shown that precipitation could be inhibited in nanopores compared to larger pores,[51,52] which would allow the pores, if interconnected, to provide an open fluid pathway during the reaction before their reequilibration.

The porosity of the aragonite dataset could not be analysed, however information about reaction pathways could still be deduced, implying interconnected pathways must have existed. The analysis of the replacement layer on the sample surface, which occurred without help of nearby fracturing, shows that the porosity in this layer is probably connected as the thickness of this layer increased through time (Fig. S5†), which requires a fluid pathway to be opened. The respective molar volumes of aragonite (34.15 $cm^3\ mol^{-1}$) and otavite (33.97 $cm^3\ mol^{-1}$)[21] are extremely close and not optimal for porosity creation. Although the porosity seems connected, it was not the principal fluid pathway used by the reaction to proceed through the aragonite sample. The replacement of aragonite by a $(Ca,Cd)CO_3$ solid solution leads to reaction-induced fracturing of the material as visible in Fig. 5(A) where fractures cross the sample in a hierarchical manner despite their absence from the starting material. These fractures could have been caused by stresses at the reaction interface with the precipitation of the new phase with a different crystallographic orientation as there was no increase in molar volume which could have created internal stress in the aragonite crystals. Another explanation for the presence of reaction-induced fracturing has been highlighted by Monasterio-Guillot *et al.* (2021),[53] who suggest that the pressure exerted by crystallization of a mineral at the surface of another mineral can lead to a build up of stress sufficient to induce fracturing of the material. It was observed that the precipitation of Na-phillipsite in etch pit edges and cracks of their host material's surface created enough stress to cause fracturing. It is possible that the presence of defects on our aragonite samples, caused during their preparation, could potentially have acted as favourable precipitation sites for otavite crystals. In the case where the supersaturation reached at the surface of our samples was high enough, the precipitation of otavite would have led to the accumulation of stress and fracturing of the aragonite crystals. These fractures opened new fluid pathways and promoted higher reaction rates, which explains why more replacement is observed inside the sample compared to the more limited replacement happening on the sample surface. After the initial surface reaction and appearance of the primary

fractures from the sample surface, the aragonite reacts further with the solution and is replaced by the solid solution phase, leading to the formation of secondary fractures that keep providing new pathways for the fluid. This fracturing network, in addition to the porosity present in the newly precipitated phase, enables the fluid to reach the centre of the samples.[40,44] This reaction-induced fracturing-driven replacement process also explains the behaviour of the reaction progress in the aragonite samples displayed in Fig. 3. The reaction advances faster with time, which is the case for a transport-driven process and is due to the decrease of the distance between unreacted material and bulk fluid when fractures appear.[40]

The replacement of $CaCO_3$ by $(Ca,Cd)CO_3$ is limited by the transport of cadmium from the bulk fluid to the reaction interface. As observed by Julia *et al.*[21] in the Carrara marble samples reacted in cadmium solutions, the cadmium concentration in the $(Ca,Cd)CO_3$ solid solution was lower close to the reaction interface and in the grain boundaries than in the bulk of the reacted volume. This observation has been explained by the kinetic limitations on the equilibration of a solution inside the restricted volume of the sample porosity with the bulk solution, leading to a reduction of cadmium in the solution at the reaction interface. This process could explain the slower reaction rate for Carrara marble compared to aragonite. The fluid needs to proceed through the porosity and grain boundaries in the Carrara marble cubes. This restricted space, also associated with the possibility of cadmium complexes attaching to the pore surfaces, could simultaneously slow down fluid transport and hence the dissolution reaction,[54] and would slow down the equilibration of the fluid inside the sample with the bulk fluid. Effectively this is a kinetically controlled reaction. Moreover, the porosity evolves during the reaction and it is possible that a partial disconnection of the pores takes place even before the cooling process and analysis of the samples, reducing the fluid mobility inside the sample. On the other hand, the aragonite samples underwent reaction-induced fracturing, leading to the creation of new and wider fluid pathways that could be replenished from the bulk fluid quickly after their formation. The fluid at the reaction interface would then have a composition closer to the bulk fluid than in the case of Carrara marble, avoiding evolved equilibration and the slowing down of the reaction. Moreover calcite and otavite present an excellent epitaxy[22] and the precipitation of a partially pore free otavite layer on some parts of the calcite surface at the reaction interface could contribute to the slow reaction rate observed.

X-ray tomography as an analytical tool has many advantages, enabling the observation of the whole sample instead of extrapolating results from two-dimensional slices and introducing a time dimension in the analysis. The reaction quantification in this study is made easier and more precise using three-dimensional tomograms as the samples can present specificities and irregularities, which can impact extrapolation from two-dimensional slices. This is especially important for the aragonite samples as the replacement proceeds mainly through reaction-induced fracturing, a process which is hierarchical and irregular throughout the sample. In this case the analysis of the microtomography scans is a more precise and reliable way to extract information about the evolution of the reaction with time and solution concentration. Moreover, the analysis of the microtomography scans of the Carrara marble dataset was necessary to gather information about the porosity volume and connectivity. This analysis allowed the interpretation of a probable closure of the porosity after termination of the reaction and showed that the amount and size of the porosity were similar in all samples. However, the analysis of X-ray microtomography scans has some limitations, mainly due to the segmentation method used, with the omission of nanoporosity (with a diameter lower than 100 nm) in the segmentation as well as the difficulty to extract porosity information in the aragonite dataset because of the limited resolution of the scan and sample specificities, such as grey level difference between the phases or interferences during imaging. Nanoporosity can have a strong impact on the permeability and reactivity of a material as constrained volume modifies the dissolution/precipitation behaviour of minerals.[49] Some recent studies have developed new techniques to extract information on porosity distribution and connectivity using two-dimensional images of the samples and using these to model the porosity,[55,56] which could be of interest for further studies of the $CaCO_3$ to $(Ca,Cd)CO_3$ replacement in cadmium-solutions. X-ray microtomography also provides important time-related information on the process, such as the acceleration of aragonite replacement with time, which is consistent with a reaction-induced fracturing replacement pathway. Moreover, although not possible in the case of this study, other studies observing reactions in minerals through time used dynamic imaging of their samples by imaging the same sample *in situ* at discrete time steps throughout the reaction.[57,58] By doing so, studies can be emancipated from the variations due to the specificities of natural samples, such as grain size variation, inclusions, and defects, and hence observe the evolution of a reaction with greater precision.

Conclusion

The present study enables a comparison of the efficiency of the replacement of $CaCO_3$ by $(Cd,Ca)CO_3$ solid solutions for Carrara marble and aragonite. Observations showed that aragonite reacts faster in cadmium-containing solutions than Carrara marble due to the reaction-driven fracturing process occurring in the samples that provides new and efficient pathways for fluid infiltration and subsequent reaction. Both datasets showed that the newly formed phase contained porosity. Overall, the porosity in the replaced phase was shown to provide a pathway for the fluid in both aragonite and Carrara marble samples as reaction progress could be observed. However, the aragonite dataset showed that reaction-induced fracturing could create a more efficient fluid pathway and could increase reaction rates with time due to the multiplication of the fracture network through the progression of the reaction. This study shows that $CaCO_3$ as aragonite can act as an effective sink for cadmium-contaminated fluids and consequently be beneficial for water decontamination. However both aragonite and Carrara marble were able to effectively sequester cadmium. The

reactions presented in this paper require high temperature and pressure, and so are applicable to industrial decontamination. Under environmental low temperature and pressure conditions, we suggest that as calcite and aragonite solubilities decrease with temperature, the reaction could also provide an efficient decontamination strategy in natural settings. The impact of the reaction-driven fracturing in aragonite could be modified by the pressure and temperature changes and thus, similar reactions should be investigated at lower temperature and pressure in order to assess their efficiency for environmental remediation.

Data availability

Additional data such as X-ray diffraction spectra of starting materials, Back-scattered electron images of reacted samples, images of measurement methods applied on the aragonite tomographs and a figure showing the pore size distribution in the Carrara marble samples are available in the ESI.† The tomographs of both datasets are available on the repository ScienceDB: Maude Julia, Christine V. Putnis, François Renard, *et al.* Tomographs of Carrara marble samples reacted in cadmium chloride solution at 200 °C[DS/OL]. V1. Science Data Bank, 1[2024-08-15]. **https://cstr.cn/31253.11.sciencedb.11705**. CSTR:31253.11.sciencedb.11705. Maude Julia, Christine V. Putnis, Oliver Plümper, *et al.* Tomographs of aragonite samples reacted in cadmium chloride solution at 200 °C[DS/OL]. V1. Science Data Bank, 2024[2024-08-15]. **https://cstr.cn/31253.11.sciencedb.11915**. CSTR:31253.11.sciencedb.11915.

Conflicts of interest

The authors have no conflicts of interest to declare.

Acknowledgements

We thank Elodie Boller at the European Synchrotron Radiation Facility for the acquisition of the X-ray tomograms of the Carrara marble samples. We also thank Yuntao Ji for the acquisition of X-ray tomograms of the aragonite samples at Utrecht University. Additionally we thank Maik Trogisch in the preparation workshop of the Institut für Mineralogie, University of Münster, for his careful sample preparation enabling tomography and SEM analyses. This project received funding from the European Union's Horizon 2020 research and innovation programme under the Marie Skłodowska-Curie initial training network (FluidNET) grant agreement No. 956127. This project also received extra funding from the H2020 EXCITE project (grant agreement no. 101005611) for Transnational Access conducted at the MINT facility at Utrecht University for the aragonite dataset X-ray tomogram acquisition.

References

1 S. V. Mohan, P. Nithila and S. J. Reddy, *J. Environ. Sci. Health, Part A: Environ. Sci. Eng. Toxic Hazard. Subst. Control*, 1996, **31**, 283–289.
2 O. Morton-Bermea, E. Hernández-Álvarez, G. González-Hernández, F. Romero, R. Lozano and L. E. Beramendi-Orosco, *J. Geochem. Explor.*, 2009, **101**, 218–224.
3 A. S. Mohammed, A. Kapri and R. Goel, in *Biomanagement of Metal-Contaminated Soils*, ed. M. S. Khan, A. Zaidi, R. Goel and J. Musarrat, Springer Netherlands, Dordrecht, 2011, vol. 20, pp. 1–28.
4 Z. Li, Z. Ma, T. J. Van Der Kuijp, Z. Yuan and L. Huang, *Sci. Total Environ.*, 2014, **468–469**, 843–853.
5 M. A. Khan, S. Khan, A. Khan and M. Alam, *Sci. Total Environ.*, 2017, **601–602**, 1591–1605.
6 Q. Yang, Z. Li, X. Lu, Q. Duan, L. Huang and J. Bi, *Sci. Total Environ.*, 2018, **642**, 690–700.
7 *Phosphorus in Agriculture: 100 % Zero*, ed. E. Schnug and L. J. De Kok, Springer Netherlands, Dordrecht, 2016.
8 G. M. Filippelli, *Elements*, 2008, **4**, 89–95.
9 S. R. Gislason and E. H. Oelkers, *Science*, 2014, **344**, 373–374.
10 F. Di Lorenzo, G. Cametti, D. Vanhecke and S. V. Churakov, *Cryst. Growth Des.*, 2020, **20**, 6157–6169.
11 A. Godelitsas, J. M. Astilleros, K. Hallam, S. Harissopoulos and A. Putnis, *Environ. Sci. Technol.*, 2003, **37**, 3351–3360.
12 R. J. Reeder, G. M. Lamble and P. A. Northrup, *Am. Mineral.*, 1999, **84**, 1049–1060.
13 C. V. Putnis, F. Renard, H. E. King, G. Montes-Hernandez and E. Ruiz-Agudo, *Environ. Sci. Technol.*, 2013, **47**, 13469–13476.
14 F. Renard, A. Røyne and C. V. Putnis, *Geosci. Front.*, 2019, **10**, 17–27.
15 F. Renard, G. Montes-Hernandez, E. Ruiz-Agudo and C. V. Putnis, *Chem. Geol.*, 2013, **340**, 151–161.
16 F. Renard, C. V. Putnis, G. Montes-Hernandez, E. Ruiz-Agudo, J. Hovelmann and G. Sarret, *Geochim. Cosmochim. Acta*, 2015, **159**, 61–79.
17 F. Renard, C. V. Putnis, G. Montes-Hernandez, H. E. King, G. D. Breedveld and G. Okkenhaug, *Environ. Sci. Technol.*, 2018, **52**, 107–113.
18 M. G. Guren, C. V. Putnis, G. Montes-Hernandez, H. E. King and F. Renard, *Chem. Geol.*, 2020, **552**, 119770.
19 V. G. R. Chada, D. B. Hausner, D. R. Strongin, A. A. Rouff and R. J. Reeder, *J. Colloid Interface Sci.*, 2005, **288**, 350–360.
20 J. A. Gómez del Río, P. J. Morando and D. S. Cicerone, *J. Environ. Manage.*, 2004, **71**, 169–177.
21 M. Julia, C. V. Putnis, H. E. King and F. Renard, *Chem. Geol.*, 2023, **621**, 121364.
22 C. Pérez-Garrido, L. Fernández-Díaz, C. M. Pina and M. Prieto, *Surf. Sci.*, 2007, **601**, 5499–5509.
23 S. L. Riechers, K. M. Rosso and S. N. Kerisit, *J. Phys. Chem. C*, 2017, **121**, 5012–5019.
24 S. L. Riechers and S. N. Kerisit, *Cryst. Growth Des.*, 2018, **18**, 159–170.
25 J. M. Zachara, C. E. Cowan and C. T. Resch, *Geochim. Cosmochim. Acta*, 1991, **55**, 1549–1562.
26 S. J. Köhler, P. Cubillas, J. D. Rodríguez-Blanco, C. Bauer and M. Prieto, *Environ. Sci. Technol.*, 2007, **41**, 112–118.
27 A. Kubier, R. T. Wilkin and T. Pichler, *Appl. Geochem.*, 2019, **108**, 104388.

28 L. Järup and A. Åkesson, *Toxicol. Appl. Pharmacol.*, 2009, **238**, 201–208.
29 K. Aoshima, *Soil Sci. Plant Nutr.*, 2016, **62**, 319–326.
30 G. F. Nordberg, A. Åkesson, K. Nogawa and M. Nordberg, in *Handbook on the Toxicology of Metals*, Elsevier, 2022, pp. 141–196.
31 World Health Organization, *Exposure to Cadmium: A Major Public Health Concern*, 2010, WHO/CED/PHE/EPE/19.4.3.
32 M. Uchimiya, *ACS Sustainable Chem. Eng.*, 2014, **2**, 2019–2027.
33 L. Lei, X. Cui, C. Li, M. Dong, R. Huang, Y. Li, Y. Li, Z. Li and J. Wu, *Chemosphere*, 2022, **286**, 131684.
34 K. Pollok, C. V. Putnis and A. Putnis, *Am. J. Sci.*, 2011, **311**, 211–236.
35 E. T. Pedrosa, C. V. Putnis and A. Putnis, *Chem. Geol.*, 2016, **425**, 1–11.
36 C. V. Putnis, K. Tsukamoto and Y. Nishimura, *Am. Mineral.*, 2005, **90**, 1909–1912.
37 S. J. Freij, A. Putnis and J. M. Astilleros, *J. Cryst. Growth*, 2004, **267**, 288–300.
38 E. Königsberger, R. Hausner and H. Gamsjäger, *Geochim. Cosmochim. Acta*, 1991, **55**, 3505–3514.
39 Q. Wang and N. H. de Leeuw, *Mineral. mag.*, 2008, **72**, 525–529.
40 B. Jamtveit, C. V. Putnis and A. Malthe-Sørenssen, *Contrib. Mineral. Petrol.*, 2009, **157**, 127–133.
41 B. Jamtveit and Ø. Hammer, *Geochem. perspect.*, 2012, **1**, 418–432.
42 O. Plümper, A. Røyne, A. Magrasó and B. Jamtveit, *Geology*, 2012, **40**, 1103–1106.
43 F. Renard, *J. Geophys. Res.: Solid Earth*, 2021, **126**, e2020JB021451.
44 C. Perdikouri, S. Piazolo, A. Kasioptas, B. C. Schmidt and A. Putnis, *Eur. J. Mineral.*, 2013, **25**, 123–136.
45 D. L. Parkhurst and C. A. J. Appelo, *User's Guide to PHREEQC (Version 2) : a Computer Program for Speciation, Batch-Reaction, One-Dimensional Transport, and Inverse Geochemical Calculations*, 1999.
46 A. Mirone, E. Brun, E. Gouillart, P. Tafforeau and J. Kieffer, *Nucl. Instrum. Methods Phys. Res., B*, 2014, **324**, 41–48.
47 S. Berg, D. Kutra, T. Kroeger, C. N. Straehle, B. X. Kausler, C. Haubold, M. Schiegg, J. Ales, T. Beier, M. Rudy, K. Eren, J. I. Cervantes, B. Xu, F. Beuttenmueller, A. Wolny, C. Zhang, U. Koethe, F. A. Hamprecht and A. Kreshuk, *Nat. Methods*, 2019, **16**, 1226–1232.
48 C. L. Christ, P. B. Hostetler and R. M. Siebert, *J. Res. U.S. Geol. Surv.*, 1974, **2**, 175–184.
49 L. H. Filiberto, C. V. Putnis and M. Julia, *Contrib. Mineral. Petrol.*, 2023, **178**, 53.
50 L. Jonas, T. John, H. E. King, T. Geisler and A. Putnis, *Earth Planet. Sci. Lett.*, 2014, **386**, 64–74.
51 B. Jamtveit, M. Kobchenko, H. Austrheim, A. Malthe-Sørenssen, A. Røyne and H. Svensen, *J. Geophys. Res.*, 2011, **116**, B12204.
52 A. G. Stack, A. Fernandez-Martinez, L. F. Allard, J. L. Bañuelos, G. Rother, L. M. Anovitz, D. R. Cole and G. A. Waychunas, *Environ. Sci. Technol.*, 2014, **48**, 6177–6183.
53 L. Monasterio-Guillot, A. Fernandez-Martinez, E. Ruiz-Agudo and C. Rodriguez-Navarro, *Geochim. Cosmochim. Acta*, 2021, **304**, 258–280.
54 W. Stumm, *Colloids Surf., A*, 1997, **120**, 143–166.
55 H. Amiri, H. Vogel and O. Plümper, *J. Geophys. Res.: Mach. Learn. Comput.*, 2024, **1**, e2024JH000178.
56 A. Chogani and O. Plümper, *Contrib. Mineral. Petrol.*, 2023, **178**, 78.
57 F. Marone, C. M. Schlepütz, S. Marti, F. Fusseis, A. Velásquez-Parra, M. Griffa, J. Jiménez-Martínez, K. J. Dobson and M. Stampanoni, *Front. Earth Sci.*, 2020, **7**, 346.
58 C. Noiriel and F. Renard, *C. R. Geosci.*, 2022, **354**, 255–280.